Studies of differential and total photoionization cross sections of carbon dioxide

Robert R. Lucchese and Vincent McKoy
Arthur Amos Noyes Laboratory of Chemical Physics, California Institute of Technology, Pasadena, California 91125
(Received 9 October 1981)

The photoionization of CO_2 has been studied using accurate frozen-core Hartree-Fock final-state wave functions. The Hartree-Fock continuum equations were solved using the iterative Schwinger variational method. We present differential and total cross sections for photoionization leading to the $X\,^2\Pi_g$, $A\,^2\Pi_u$, $B\,^2\Sigma_u^+$, and $C\,^2\Sigma_g^+$ states of CO_2^+ as well as for oxygen and carbon K-shell photoionization. The present cross sections are compared to experimental data and are found to be in generally good agreement. The theoretical cross sections exhibit features due to a narrow shape resonance in those channels where the continuum wave functions have σ_u symmetry. The relation between these results and experimental cross sections is discussed. The present fixed-nuclei results have also been compared to published theoretical results obtained using the Stieltjes-Tchebycheff moment theory approach and the continuum multiple-scattering method.

I. INTRODUCTION

Several recent theoretical studies have investigated the partial-channel photoionization cross sections and photoelectron angular distributions of carbon dioxide. They include the comprehensive work by Padial *et al.*[1] which employed the Stieltjes-Tchebycheff moment theory (STMT) approach to obtain photoionization cross sections, and the studies of Swanson *et al.*[2,3] which used the continuum multiple-scattering method (CMSM) to compute both cross sections and photoelectron angular distributions. Both the CMSM and STMT approaches obtained photoionization cross sections within a Hartree-Fock final-state framework. The present study is directed at obtaining accurate Hartree-Fock final-state continuum wave functions which are then used to compute both differential and integral photoionization cross sections. Comparison of the present results with available experimental data and with the results of the STMT and CMSM methods allows us to examine the accuracy of the Hartree-Fock final-state model and the utility of the STMT and CMSM methods.

The theoretical approach used here is identical to the approach used in an earlier study of the photoionization of N_2.[4] We have used the fixed-nuclei approximation with the final-state photoionization wave function computed in the frozen-core Hartree-Fock (FCHF) approximation. To study initial-state correlation effects, we have computed the photoionization cross section using both a Hartree-Fock (HF) initial-state wave function and a configuration interaction (CI) initial-state wave function. The FCHF final-state wave functions were obtained using the iterative Schwinger variational method,[5–7] which we found to be an effective approach for obtaining HF continuum solutions in our study of the photoionization of N_2.[4]

We have studied the photoionization of CO_2 from the valence molecular orbitals ($1\pi_g$, $1\pi_u$, $3\sigma_u$, and $4\sigma_g$) and from the K-shell orbitals ($1\sigma_g$, $1\sigma_u$, and $2\sigma_g$). Of particular interest in this system are the narrow-shape resonances which occur for continuum solutions of σ_u symmetry.[2,3,8–10] Such shape resonances can lead to an enhancement in the photoionization cross section, marked changes in the photoelectron angular-distribution, and non-Franck-Condon vibrational effects.

We compare our valence-shell photoionization cross sections of CO_2 to the $(e,2e)$ cross sections of Brion and Tan,[11] to the synchrotron source cross sections of Gustafsson *et al.*,[12] and to the fluorescence cross sections of Lee *et al.*[13] and Carlson *et al.*[14] The carbon K-shell cross sections are compared to the electron energy-loss data of Wight and Brion[15] and the oxygen K-shell cross sections to the photoabsorption cross sections of Barrus *et al.*[16] We also compare our asymmetry parameters with the experimental data of Katsumata *et al.*,[17] of Carlson *et al.*,[18(a)] and of Grimm *et al.*[18(b)] We find good agreement between experimental data

and the present theoretical results. There are, however, two noticeable disagreements. The first major disagreement is the lack of experimental observation of the computed resonant enhancement of the photoionization cross section leading to the $C\,^2\Sigma_g^+$ state of CO_2^+. However, the experimentally determined asymmetry parameters of Carlson *et al.*[18] do lend support to the existence and to the predicted position of this shape resonance. The second area of disagreement is that the experimental cross section has a peak at a photon energy of 21 eV, which is not obtained in the present results. We have tentatively attributed this discrepancy to the effects of autoionization which have not been included here.

We also compare our results to the published results of the STMT[1] and CMSM[2,3] methods. In a previous paper[9] we discussed the relationship between the results of the Schwinger method used here and the results of the STMT and CMSM methods for photoionization leading to the $C\,^2\Sigma_g^+$ state of CO_2^+. In the present paper we compare the results of the Schwinger method with those of the STMT and the CMSM method leading to other states of CO_2^+. As in the case of the $C\,^2\Sigma_g^+$ channel discussed in the earlier paper,[9] we find that the STMT method as applied by Padial *et al.*[1] does not reliably predict the cross section in the region of narrow-shape resonances found in the photoionization of CO_2. Also due to limitations of the computer program used by Padial *et al.*[1] the incorrect HF potentials were used in the calculations of the $\pi\rightarrow\delta$ partial-channel contributions. This led to somewhat different results than those obtained here using the correct HF potential. We have also compared our results with the CMSM results of Swanson *et al.*[2,3] As indicated in Ref. 9 we find that the CMSM method does show the narrow-shape resonances found here, but the resonant CMSM cross sections are too large by a factor of about 2 and the positions of the resonances are at different energies than found here.

II. METHOD

A. Final-state wave functions

The final-state photoionization wave functions used in this study were obtained using the FCHF approximation. In the FCHF model the final-state wave function is described by a single electronic configuration in which the ionic core orbitals are constrained to be identical to the HF orbitals of the neutral molecule. The Lippmann-Schwinger equation for the remaining continuum electron is (in atomic units)

$$\Psi_{\vec{k}}^{(\pm)}=\Psi_{\vec{k}}^{(\pm)}+G^{c(\pm)}U\Psi_{\vec{k}}^{(\pm)}\,, \tag{1}$$

with $U(\vec{r})=2V(\vec{r})$, where $V(\vec{r})$ is the appropriate short-range potential describing the scattering process and $G^{c(\pm)}$ is the Coulomb Green's function defined by

$$G^{c(\pm)}=(\nabla^2+\frac{2}{r}+k^2\pm i\epsilon)^{-1}\,. \tag{2}$$

In Eq. (1), $\Psi_{\vec{k}}^{c(\pm)}$ is a pure Coulomb scattering function. In the FCHF approximation, V is a generalized Phillips-Kleinman pseudopotential[19] which constrains the continuum orbital to be orthogonal to the occupied molecular orbitals. For photoionization from the nth (nondegenerate) orbital of a closed-shell molecule containing n doubly occupied molecular orbitals, the potential V is given by[4]

$$V=V^{\rm SE}-LQ-QL+QLQ+\frac{1}{r}\,, \tag{3}$$

where

$$L=-\frac{1}{2}\nabla^2-\frac{k^2}{2}+V^{\rm SE}\,, \tag{4}$$

$$Q=\sum_{i=1}^{n}|\phi_i\rangle\langle\phi_i|\,, \tag{5}$$

and $V^{\rm SE}$ is the static-exchange potential

$$V^{\rm SE}=\sum_{i=1}^{n-1}(2J_i-K_i)+J_n+K_n-\sum_{\alpha}\frac{Z_\alpha}{r_{i\alpha}}\,. \tag{6}$$

In Eq. (6), the functions ϕ_i are the n molecular orbitals, Z_α is the nuclear charge of the αth nucleus, and J_i and K_i are the usual Coulomb and exchange operators.[20]

We solve the Lippmann-Schwinger equation using the iterative Schwinger variational method which has been described in detail elsewhere.[4–7] Using this iterative method, the continuum solution at the nth iteration is expanded in a partial-wave series

$$\Psi_{\vec{k}}^{(-)S_n}(\vec{r})=\left[\frac{2}{\pi}\right]^{1/2}\sum_{l=0}^{l_p}\sum_{m=-l}^{+l}i^l\psi_{klm}^{(-)S_n}(\vec{r})Y_{lm}^*(\Omega_{\hat{k}})\,, \tag{7}$$

where an infinite sum over l's has been truncated at $l=l_p$. The set of partial-wave scattering solutions at the nth iteration,

$$S_n=\{\psi_{kl_1m}^{S_n},\ldots,\psi_{kl_pm}^{S_n}\}\,, \tag{8}$$

is obtained from the previous set of solutions, S_{n-1}, using

$$\psi_{klm}^{(-)S_n}(\vec{r})=\phi_{klm}^{c(-)}(\vec{r})+\sum_{\chi_i,\chi_j\in R\cup S_{n-1}}\langle\vec{r}\,|\,G^{c(-)}U\,|\,\chi_i\rangle[D^{-1}]_{ij}\langle\chi_j\,|\,U\,|\,\phi_{klm}^{c(-)}\,, \tag{9}$$

where $[D^{-1}]_{ij}$ is the matrix inverse of

$$D_{ij}=\langle\chi_i\,|\,U-UG^{c(-)}U\,|\,\chi_j\rangle\,. \tag{10}$$

The set of functions R in Eq. (9) is composed of L^2 functions, which, in the present study, are taken to be spherical Gaussian functions defined by

$$\chi^{\alpha,l,m,\vec{A}}(\vec{r})=N_{\alpha lm}\,|\,\vec{r}-\vec{A}\,|^{l}e^{-\alpha|\vec{r}-\vec{A}|^2}\times Y_{lm}(\Omega_{\vec{r}-\vec{A}})\,. \tag{11}$$

The L^2 basis sets R for the various scattering symmetries are given in Tables I and II. Note that in Eq. (9) the set of functions S_{-1} is taken to be the null set. When the wave functions given by this iterative scheme do converge, it can be shown that they are solutions of the Lippmann-Schwinger equation given in Eq. (1).[5]

These continuum solutions are then used to compute photoionization cross sections. The cross section for ionization of an initial bound state Ψ_i to the continuum state $\Psi_{f,\vec{k}}$ by linearly polarized light is given in the dipole length approximation by

$$\frac{d^2\sigma^L}{d\Omega_{\hat{k}}d\Omega_{\hat{n}}}=\frac{4\pi^2E}{c}k\,|\,\langle\Psi_i\,|\,\vec{r}\cdot\hat{n}\,|\,\Psi_{f,\vec{k}}^{(-)}\rangle\,|^2\,, \tag{12}$$

and in the dipole velocity approximation by

$$\frac{d^2\sigma^V}{d\Omega_{\hat{k}}d\Omega_{\hat{n}}}=\frac{4\pi^2}{cE}k\,|\,\langle\Psi_i\,|\,\vec{\nabla}\cdot\hat{n}\,|\,\Psi_{f,\vec{k}}^{(-)}\rangle\,|^2\,, \tag{13}$$

where E is the photon energy, $\hat{n}$ is the direction of

TABLE I. Scattering basis sets of σ symmetry used in the Schwinger variational expression.[a]

Number of functions	Center	l	m	Exponents[b]
		$1\sigma_u,3\sigma_u\rightarrow k\sigma_g$		
7	O	0	0	32.0−0.5
5	O	1	0	8.0−0.5
3	O	2	0	2.0−0.5
7	C	0	0	32.0−0.5
5	C	2	0	8.0−0.5
3	C	4	0	2.0−0.5
		$1\pi_u\rightarrow k\sigma_g$		
6	O	0	0	32.0−1.0
4	O	1	0	8.0−1.0
2	O	2	0	2.0, 1.0
2	O	3	0	2.0, 1.0
2	O	4	0	2.0, 1.0
1	O	5	0	1.0
6	C	0	0	32.0−1.0
4	C	2	0	8.0−1.0
2	C	4	0	2.0, 1.0
2	C	6	0	1.0, 0.5
1	C	8	0	0.5
		$1\sigma_g,2\sigma_g,4\sigma_g,1\pi_g\rightarrow k\sigma_u$		
7	O	0	0	32.0−0.5
5	O	1	0	8.0−0.5
3	O	2	0	2.0−0.5
7	C	1	0	32.0−0.5
5	C	3	0	8.0−0.5
3	C	5	0	2.0−0.5

[a]These basis sets are composed of spherical Gaussian functions as defined in Eq. (11) and correspond to the set R of Eq. (9). [b]The notation 32.0−0.5 denotes a geometric series of exponents starting with 32.0 and ending with 0.5 with a ratio between succesive exponents of 2.0.

TABLE II. Scattering basis sets of π and δ symmetry used in the Schwinger variational expression.[a]

Number of functions	Center	l	m	Exponents
		$1\sigma_u,3\sigma_u,1\pi_u\rightarrow k\pi_g$		
6	O	1	1	16.0−0.5
5	O	2	1	8.0−0.5
5	C	2	1	8.0−0.5
3	C	4	1	2.0−0.5
		$1\sigma_g,2\sigma_g4\sigma_g,1\pi_g\rightarrow k\pi_u$		
6	O	1	1	16.0−0.5
5	O	2	1	8.0−0.5
5	C	1	1	8.0−0.5
3	C	3	1	2.0−0.5
		$1\pi_u\rightarrow k\delta_g$		
5	O	2	2	8.0−0.5
3	O	3	2	2.0−0.5
2	O	4	2	1.0, 0.5
5	C	2	2	4.0−0.25
3	C	4	2	1.0−0.25
3	C	6	2	1.0−0.25
		$1\pi_g\rightarrow k\delta_u$		
5	O	2	2	8.0−0.5
3	O	3	2	2.0−0.5
4	C	3	2	4.0−0.5
2	C	5	2	1.0, 0.5

[a]See notes of Table I.

the polarization of the light, c is the speed of light, and $\vec{k}$ is the asymptotic momentum of the photoelectron. When these cross sections are averaged over all possible orientations of the molecule in the laboratory frame, the resulting differential cross section is of the form

$$\frac{d\sigma^{L,V}}{d\Omega_{\hat{k}}}=\frac{\sigma^{L,V}}{4\pi}[1+\beta_{\hat{k}}^{L,V}P_2(\cos\theta)]\ , \tag{14}$$

where θ is the angle between the direction of polarization of the light and the momentum of the photoelectron. For all channels considered in this study we have computed both the total cross section $\sigma^{L,V}$ and the asymmetry parameters $\beta_{\hat{k}}^{L,V}$.

To compute the final-state continuum wave functions we must evaluate the various matrix elements given in Eq. (9). We have used a single-center expansion approach to evaluate all such matrix elements. In actual scattering calculations we use standing-wave boundary conditions, thus allowing radial wave functions to be represented by real-valued functions. We define our partial-wave expansion parameters as follows:

(1) l_m = maximum l included in the expansion of scattering functions [χ_i's of Eq. (9)], of the Coulomb Green's function and of the projection orbitals [ϕ_i of Eq. (5)];
(2) $l_s^{\rm ex}$= maximum l included in the scattering functions in the exchange terms;
(3) $l_i^{\rm ex}$= maximum l included in the expansion of the occupied orbitals in the exchange terms;
(4) $l_i^{\rm dir}$= maximum l included in the expansion of the occupied orbitals in the direct potential;
(5) $\lambda_m^{\rm ex}$= maximum l included in the expansion of $1/r_{12}$ in the exchange terms;
(6) $\lambda_m^{\rm dir}$= maximum l included in the expansion of $1/r_{12}$ in the direct potential.

As usual we have included nuclear potential terms up to $\lambda=2l_m$. We have expanded all radial integrals on a grid of 1000 points extending out to $r=90$ a.u. The smallest step size in the grid was 0.005 a.u., which was used for points within 0.1 a.u. of the nuclei. A step size of 0.01 a.u. was used for all other points out to $r=3.0$ a.u. The largest step size in the remainder of the grid was 0.16 a.u.

In studying the convergence of the single-center method we fixed some of the expansion parameters. We have taken $l_i^{\rm dir}=59$, $l_s^{\rm ex}=l_m$, and $\lambda_m^{\rm dir}=2l_m$. We also fixed $l_i^{\rm ex}$ to be $l_i^{\rm ex}=38(1\sigma_g)$, $10(2\sigma_g)$, $24(3\sigma_g)$, $16(4\sigma_g)$, $39(1\sigma_u)$, $23(2\sigma_u)$, $15(3\sigma_u)$, $15(1\pi_u)$, $16(1\pi_g)$. These values for $l_i^{\rm ex}$ correspond to having normalized the expansions of the various orbitals to better than 0.99. The value for l_p of Eq. (7) was fixed at $l_p=10$.

Thus we have only retained two independent parameters, l_m and $\lambda_m^{\rm ex}$, to define the single-center expansion. To study the convergence of the static-exchange potential of CO_2, we have considered five combinations of values of l_m and $\lambda_m^{\rm ex}$:

(A) $l_m=59$, $\lambda_m^{\rm ex}=40$;
(B) $l_m=55$, $\lambda_m^{\rm ex}=40$;
(C) $l_m=51$, $\lambda_m^{\rm ex}=40$;
(D) $l_m=47$, $\lambda_m^{\rm ex}=40$;
(E) $l_m=59$, $\lambda_m^{\rm ex}=30$.

We have used these five sets of parameters to compute the energy of the peak cross section of the resonant $4\sigma_g\rightarrow k\sigma_u$ photoionization channel of CO_2. The peak energy of such a shape resonance is a sensitive test of the convergence of these parameters. The peak energies were obtained from a zero-iteration calculation ($n=0$) using Eq. (9). The resulting peak photon energies were, $E_{\rm max}^A=41.79$ eV, $E_{\rm max}^B=41.85$ eV, $E_{\rm max}^C=41.92$ eV, $E_{\rm max}^D=42.01$ eV, and $E_{\rm max}^E=41.82$ eV. To test the effect of the iterative procedure on these results, we performed one iteration using parameter set A and obtained a first iteration result of $E_{\rm max}^{A'}=41.79$ eV. Thus the peak energy was unchanged by one iteration and the procedure seems well converged by the first iteration. All other results presented in this paper were obtained using the results of the first iteration of Eq. (9) (i.e., using the S_1 scattering functions). In an earlier study we found empirically that the energy of the peak cross section in a σ symmetry-shape resonance converges with partial-wave expansion as

$$E^{(l_m)}-E^{(\infty)}\propto 1/l_m^3\ . \tag{15}$$

The results of parameter sets $A-D$ satisfy this relationship well with an extrapolated $E^{(\infty)}=41.57$ eV. Thus we see that parameter set A is within 0.3 eV of the fully converged result. Also, we notice that the $\lambda_m^{\rm ex}$ parameter seems to be at least as well converged at $\lambda_m^{\rm ex}=40$. Thus for all further calculations in CO_2 we have used the parameter set A.

B. Initial-state wave functions

We have studied the effects of initial-state correlation on the photoionization cross section by cal-

culating cross sections using both a HF wave function and a CI wave function as the initial state. The HF basis set was a [3s2p 1d] contracted Cartesian Gaussian basis set.[21] With a R(C-O) bond length of 2.1944 a.u. the HF energy in this basis was $E=-187.674\,286$ a.u.

The CI initial-state wave function contained "single-plus-double exitation" type configurations. These are the only configurations which have a nonzero contribution to the photoionization cross section when the final state is computed using the FCHF approximation.[4] The virtual orbital space for the CI calculation was a restricted set of molecular orbitals from a separated-pair calculation.[20] The separated-pair wave function was of the form

$$(1\sigma_g)^2(2\sigma_g)^2(3\sigma_g)^2(4\sigma_g,6\sigma_g,4\sigma_u,6\sigma_u)^2(1\sigma_u)^2(2\sigma_u)^2(2\sigma_u)^2(3\sigma_u,5\sigma_g,5\sigma_u)^2(1\pi_{ux},3\pi_{ux},2\pi_{gx})^2(1\pi_{uy},3\pi_{uy},2\pi_{gy})^2$$
$$\times(1\pi_{gx},3\pi_{gx},2\pi_{ux})^2(1\pi_{gy},3\pi_{gy},2\pi_{uy})^2\,, \quad (16)$$

where the orbitals within each pair of parentheses represent natural orbitals of a particular pair function. Also, the orbitals in each pair function, which are doubly occupied in the HF approximation, were not allowed to vary. The energy of this separated-pair wave function for CO_2 was $E=-187.707\,766$ a.u. The CI wave function was then taken to be a linear combination of configurations constructed from the orbitals determined in the separated-pair calculation and differing from the HF configuration by no more than two orbitals. We have also restricted the calculation by requiring the $1\sigma_g$, $2\sigma_g$, and $1\sigma_u$ orbitals to remain doubly occupied in all configurations. The resulting wave function had 505 spatial configurations in D_{2h} symmetry from which 797 spin eigenfunctions were constructed. The energy of the CI wave function was $E=-187.943\,937$ a.u.

III. RESULTS AND DISCUSSION

A. Valence-shell photoionization

Of primary interest here is the photoionization from the valence orbitals of CO_2. These photoionization channels lead to the four lowest states of CO_2^+, which are the $(1\pi_g)^{-1}X\,^2\Pi_g$ state obtained by ionizing an electron from the $1\pi_g$ orbital with a vertical ionization potential (IP) of 13.8 eV, the $(1\pi_u)^{-1}A\,^2\Pi_u$ state with an IP of 17.7 eV, the $(3\sigma_u)^{-1}B\,^2\Sigma_u^+$ state with an IP of 18.2 eV, and the $(4\sigma_g)^{-1}C\,^2\Sigma_g^+$ state with an IP of 19.4 eV.[22]

In Fig. 1 we present the cross sections leading to the $X\,^2\Pi_g$ and $C\,^2\Sigma_g^+$ states of CO_2^+. Both of these channels contain narrow-shape resonances in the partial channels where the continuum orbital is of σ_u symmetry. These resonances are apparent in the computed photoionization cross sections. In the $X\,^2\Pi_g$ channel, the resonance produces a shoulder in the cross section at a photon energy of 35 eV and in the $C\,^2\Sigma_g^+$ channel the resonance produces a prominent peak in the cross section at 42 eV. In Fig. 1 we present four different theoretical cross sections for each channel. These four cross sections were obtained using the HF initial-state wave function with the dipole length (HFL) and

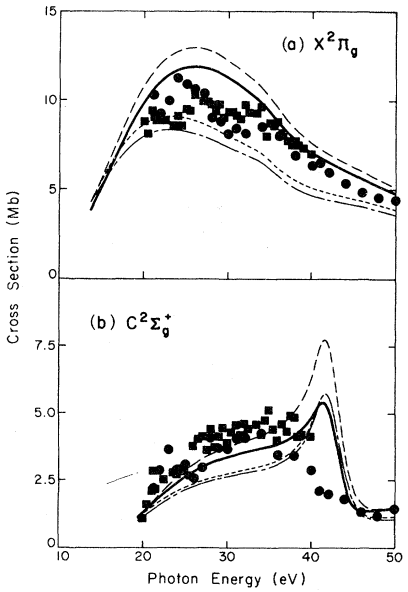

FIG. 1. Photoionization cross section for the production of the $X\,^2\Pi_g$ and $C\,^2\Sigma_g^+$ states of CO_2^+: —, present results using the dipole length approximation and the CI initial-state wave function; — - — -, present results using the dipole velocity approximation and the CI initial-state wave function; — — —, present results using the dipole length approximation and the HF initial-state wave function; - - -, present results using the dipole velocity approximation and the HF initial-state wave function; ●, experimental results of Brion and Tan (Ref. 11); ■, experimental results of Gustafsson *et al.* (Ref. 12). One megabarn (Mb) is 10^{-18} cm^2.

dipole velocity (HFV) approximations, as well as using the correlated initial-state wave function, discussed in Sec. II B, in the dipole length (CIL) and dipole velocity (CIV) approximations.

As note previously by Padial *et al.*,[1] if the correct singlet HF potential were used in obtaining the $1\pi_g \rightarrow k\pi_u$ partial-channel cross section, then the cross section would be spuriously enhanced at low photon energy. This difficulty is due to a strong $1\pi_g \rightarrow 2\pi_u$ ($n \rightarrow \pi^*$) transition which is incorrectly placed above the ionization threshold in the HF approximation. Thus we have been forced to use the triplet coupled potential to obtain the cross section in the $1\pi_g \rightarrow k\pi_u$ photoionization channel. This is the only channel where we did not use the correct singlet HF potential.

The difference between the length and velocity forms of the cross section in Fig. 1 can be viewed as an estimate of the minimum error in these calculations.[23,24] In our previous study of the photoionization of N_2 we found that, in nonresonant regions of the photoionization cross section, the inclusion of initial-state correlation tended to reduce the cross section in both the length and velocity approximations, whereas in the region of the photoionization cross section dominated by a shape resonance, the inclusion of initial-state correlation differentially lowered the length form of the cross section relative to the velocity form, bringing the two approximations into close agreement.[4] The same trends can be seen in the two channels given in Fig. 1. In the $C\,^2\Sigma_g^+$ channel, inclusion of the initial-state correlation brings the length form very close to the velocity form in the region of the resonance. In the $X\,^2\Pi_g$ channel, this effect is not as noticeable since the cross section at 35 eV is not dominated by the resonant $1\pi_g \rightarrow k\sigma_u$ partial channel.

In Fig. 1 the cross sections leading to the $X\,^2\Pi_g$ and $C\,^2\Sigma_g^+$ states are compared to the experimental data of Gustafsson *et al.*[12] and Brion and Tan.[11] The experimental results for the $X\,^2\Pi_g$ channel fall between the length and velocity estimates of the cross section, although there is no reason for this to be generally true. There also seems to be some evidence of a shoulder in the experimental cross section at a photon energy of 35 eV, as was obtained in the theoretical cross section. The $C\,^2\Sigma_g^+$ experimental cross sections do not contain any such evidence of the resonance enhancement seen theoretically. As has been noted by Swanson *et al.*,[2] both vibrational effects and final-state correlation would lower and broaden the theoretical cross section. In an earlier study,[10] we have examined the effects on this cross section of averaging the cross section over the symmetric stretch vibrational mode, and found that the peak resonant cross section was lowered by about 15%. Inclusion of vibrational effects of other modes would also be expected to lower the peak cross section. Thus the theoretical cross section using the FCHF final-state model and including averaging over all vibrational modes would probably not differ from the experimental cross section by more than a few megabarns in the region of the 42-eV resonance. However, there would still seem to be a qualitative discrepancy in this channel which may be attributed to the effects of final-state correlation.

In Fig. 2 we compare our fixed-nuclei HFL results for the $X\,^2\Pi_g$ and $C\,^2\Sigma_g^+$ channels to the cross sections given by the STMT and CMSM methods also using the fixed-nuclei dipole length form of the cross section. The STMT cross section of Padial *et al.*[1] for the $X\,^2\Pi_g$ channel agrees fairly well with the present cross section at high energy although there is no evidence of a shoulder in the STMT cross section at 35 eV. At lower photon energies there is a larger disagreement between the STMT and the present results. Most of the

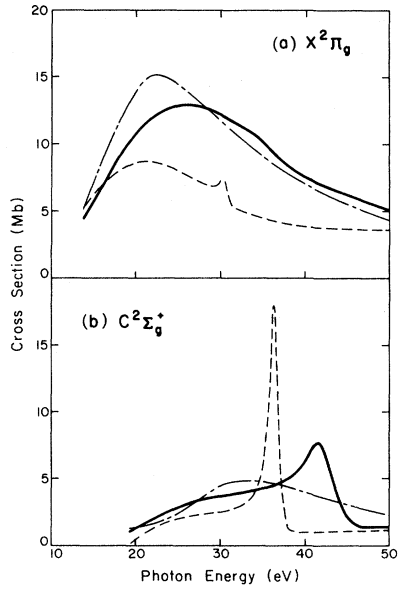

FIG. 2. Comparison of different theoretical cross sections for the production of the $X\,^2\Pi_g$ and $C\,^2\Sigma_g^+$ states of CO_2^+: —, present single-center FCHF results; — - — -, FCHF results obtained using the STMT approach (Ref. 1); — — —, fixed-nuclei CMSM results (Ref. 2).

discrepancy at low energy is due to differences in the $1\pi_g \rightarrow k\delta_u$ partial-channel cross sections. The STMT cross sections were extracted from the results of a diagonalization of the FCHF operator in a large L^2 basis set of Cartesian Gaussian basis functions. These calculations were performed using standard bound-state computer codes, which require that the interelectronic interactions be expressible in terms of the usual J and K operators.[20,25] The singlet potential appropriate to the $\pi^3\delta$ case is not expressible in terms of J and K operators when real valued molecular orbitals are used. Thus the STMT results were actually obtained using a triplet-coupled potential which can be expressed in terms of J and K operators. To show the effect of using these different HF potentials, we present in Fig. 3 the results of noniterative Schwinger calculations where both the triplet and singlet potentials have been used, and compare them to the STMT $1\pi_g \rightarrow k\delta_u$ results of Padial *et al.*[1] Thus it can be seen that a large portion of the discrepancy in the $1\pi_g \rightarrow k\delta_u$ channel is due to using the triplet potential in obtaining the STMT cross sections.

In Fig. 2(a) we also compare the Schwinger results for the $X\,^2\Pi_g$ channel to the fixed-nuclei CMSM cross section of Swanson *et al.*[2] We can see that the CMSM cross sections are generally too small and that the shape resonance in the $1\pi_g \rightarrow k\sigma_u$ partial channel is at a lower energy than that obtained using the Schwinger method. The fixed-nuclei resonant feature in the CMSM cross section is seen to be much more pronounced than the broad shoulder obtained using the Schwinger method.

In Fig. 2(b), we compare the various theoretical cross sections for the $C\,^2\Sigma_g^+$ channel. This comparison has been discussed in detail in an earlier paper.[9] Briefly, we can see that the STMT results show no evidence of a resonant enhancement of the photoionization cross section. In contrast, the results of the CMSM method show an unrealistically large and narrow resonant cross section, which differs from the present results in position by about 5 eV and in magnitude by over a factor of 2.

In Fig. 4 we present the computed asymmetry parameters for the $X\,^2\Pi_u$ and $C\,^2\Sigma_g^+$ channels. We have only presented the results which were obtained using the correlated initial-state wave function. We found that the effects of initial-state correlation on the asymmetry parameter were small, and thus we chose only to present our most accurate results. We have compared the present results with available experimental data and to the values predicted by the CMSM method.[3]

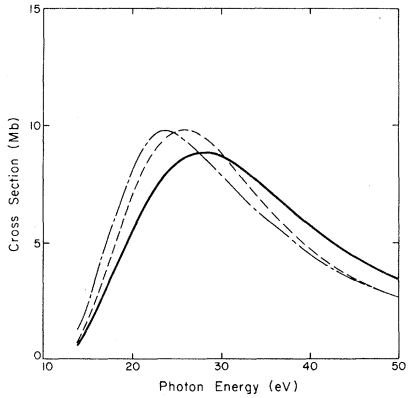

FIG. 3. Cross sections obtained using different scattering potentials in the $1\pi_g \rightarrow k\delta_u$ photoionization channel of CO_2; —, present results using correct singlet potential: — — —, present results using triplet potential; — - — -, results of STMT method (Ref. 1) using triplet potential.

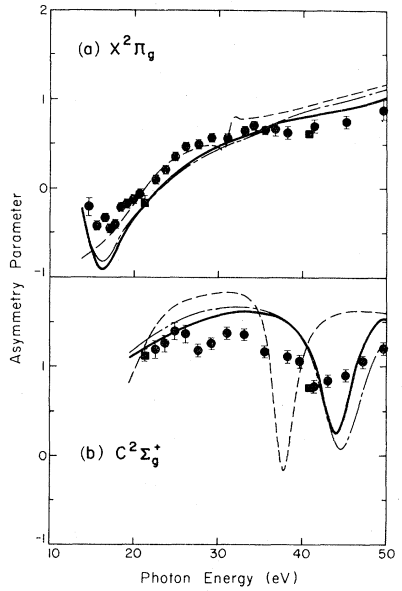

FIG. 4. Photoelectron asymmetry parameters for photoionization leading to the $X\,^2\Pi_g$ and $C\,^2\Sigma_g^+$ state of CO_2^+: —, present results using the dipole length approximation and a CI initial-state wave function; — - —-, present results using the dipole velocity approximation and a CI initial-state wave function; ---, fixed-nuclei CMSM results (Ref. 3); ●, experimental data of Grimm *et al.* (Ref. 18); ■, experimental data of Katsumata *et al.* (Ref. 17).

The resonance in the $X\,^2\Pi_g$ channel at 35 eV is barely visible as a slight bump in the dipole length asymmetry parameters. The CMSM asymmetry of Swanson *et al.*[3] are seen to have a larger resonance effect than do the present values. Both the CMSM and Schwinger results are in reasonable accord with two line-source measurements of Katsumata *et al.*,[17] and with the continuous-source measurements of Grimm *et al.*[18(b)] As can be seen in Fig. 4(b), the resonance in the $C\,^2\Sigma_g^+$ channel leads to very dramatic effects in the asymmetry parameters. The experimental results of Carlson *et al.*[18(a)] show a fairly large dip in the β values around a photon energy of 40 eV. Both the Schwinger and CMSM fixed-nuclei results overestimate the magnitude of the resonance effect. Inclusion of vibrational effects is known to make this feature shallower.[3,10] Including just the symmetric stretch vibrational mode in an earlier paper,[10] we found that vibrational averaging of the cross section reduced the dip in the asymmetry parameter by about 25%. Thus if other vibrational degrees of freedom were considered in the averaging, it would seem that the theoretical β could be in fairly good quantitative agreement with the experimental results using just the FCHF final-state approximation.

The cross sections leading to the production of the $A\,^2\Pi_u$ and $B\,^2\Sigma_u^+$ states of CO_2^+ are given in Fig. 5. We have compared our cross sections to the experimental fluorescence cross sections of Lee *et al.*[13] for the $A\,^2\Pi_u$ state, and to the fluorescence data of Carlson *et al.*[14] for the $B\,^2\Sigma_u^+$ state. We have also presented cross sections which were derived by taking the ratios of the cross sections for the A and B states obtained from the photoelectron spectra by Samson and Gardner[26] and multiplying them by the total cross section for the A and B states given by Brion and Tan.[11] The cross section for the $B\,^2\Sigma_u^+$ state is in reasonably good agreement with results obtained from fluorescence measurements, whereas the cross section for the $A\,^2\Pi_u$ state has a more serious disagreement with the experimental fluorescence data in the region of 21-eV photon energy. The limited number of photoelectron measurements available seem to indicate the reverse situation, with agreement between theory and photoelectron experiments being good in the A channel and a major disagreement in the 21-eV photon-energy range in the B channel. The comparison of the present theoretical results with the photoelectron results thus seems to indicate that near the photon energy of 21 eV, a large contribution to the correct cross section for the $B\,^2\Sigma_u^+$ channel must come from multielectron effects in the final state. One possible effect which would enhance the cross section would be autoionization due to higher-lying ionic states. The lowest multielectron ionic state which has been identified, has an IP of 23 eV and has been characterized by Domcke *et al.*[27] as being dominated by the $(1\pi_g)^{-2}(2\pi_u)$ configuration. This autoionization enhancement would be analogous to the enhancement due to the $C\,^2\Sigma_u^+$ state in the photoionization cross section of N_2, which is characterized by the $(1\pi_u)^{-1}(3\sigma_g)^{-1}(1\pi_g)$ configuration.

It is clear from Fig. 5 that the fluorescence cross section disagrees strongly with the photoelectron cross section in the region of the feature, which we suggest is due to autoionization. We can speculate that in this region there is a mechanism whereby a large fraction of the molecules, which are initially in the B state, crossover to the A state before the molecule fluoresces. Such a crossover mechanism has been suggested by Samson and Gardner[26]; however, they assumed that the crossover rate would be independent of the photon energy. As discussed by

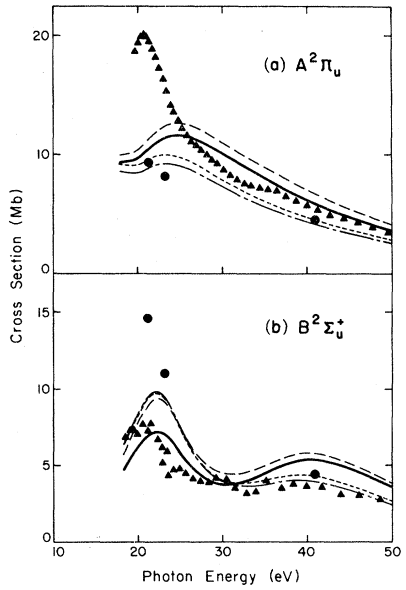

FIG. 5. Photoionization cross section for the production of the $A\,^2\Pi_u$ and $B\,^2\Sigma_u^+$ states of CO_2^+, for definitions of the lines see Fig. 1: ▲, experimental fluorescence data of Lee *et al.* (Ref. 13) for the A state and of Carlson *et al.* (Ref. 14) for the B state; ●, experimental photoelectron cross sections obtained by taking the total $A+B$ cross sections of Brion and Tan (Ref. 11) and using the A/B ratios of Samson and Gardner (Ref. 26) to compute individual A and B cross sections.

Gustafsson *et al.*,[12] such a photon-energy-independent mechanism does not agree with experimental evidence since, as can be seen in Fig. 5, at 40.8 eV the cross section derived from fluorescence and photoelectron measurements are in much better agreement than at 21.2 eV. This suggests that such a mechanism must depend on the photon energy and in particular the presence of autoionization in the cross section must strongly effect the crossover rate.

It is of interest also to note that both the $A\,^2\Pi_u$ and $B\,^2\Sigma_u^+$ channels exhibit rising eigenphase sums in the partial channels where the continuum electron has σ_g and π_g symmetry. In the case of the π_g continuum channels, these rising eigenphase sums can be atttributed to very broad resonances at about 22 eV above threshold.

The resonant increase in the eigenphase sums in the σ_g channels occurs at low energy and due to a rising eigenphase which is primarily s wave. In Fig. 6 we give both the eigenphase sums and cross sections for the $1\pi_u \rightarrow k\sigma_g$ and $3\sigma_u \rightarrow k\sigma_g$ channels. The effects of the resonancelike features on the cross sections in these two channels are markedly different, with the $1\pi_u \rightarrow k\sigma_g$ channel showing a minimum and the $3\sigma_u \rightarrow k\sigma_g$ showing a maximum in the region of interest. As can be seen in Fig. 5(b), the effect of initial-state correlation on the maximum in the $3\sigma_u \rightarrow k\sigma_g$ cross section is to increase the difference between length and velocity forms of the cross section. This effect is different from that found for cross sections dominated by shape resonances discussed earlier, where length and velocity forms are brought closer together by initial-state correlations. Thus it seems that these two σ_g photoionization continuum channels are being affected by a one-electron resonant process which is qualitatively different from the usual shape resonance, which is characterized by a rising eigenphase corresponding to a higher value of l, i.e., $l > 0$.

In Fig. 7 we compare the present Schwinger results for the $A\,^2\Pi_u$ and $B\,^2\Sigma_u^+$ channels with the cross sections obtained by Padial *et al.*[1] using the STMT method. The peak in the STMT cross section in the $A\,^2\Pi_u$ channel is shifted to a lower energy than that obtained using the Schwinger method. As was the case in the $X\,^2\Pi_g$ channel, most of the cross section comes from the $\pi \rightarrow \delta$ partial channel. The STMT results were again obtained using the triplet potential in this channel, and this may account for the shift of the peak cross section to lower energy. In the $B\,^2\Sigma_u^+$ channel both the $3\sigma_u \rightarrow k\sigma_g$ and $3\sigma_u \rightarrow k\pi_g$ features are at lower energy in the STMT cross sections. The source of these discrepancies is uncertain.

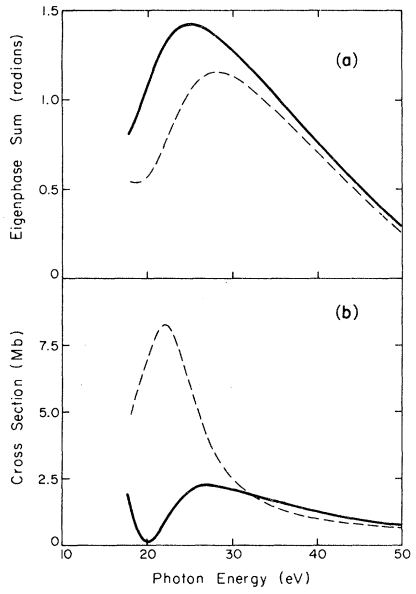

FIG. 6. Eigenphase sums and cross sections for the $1\pi_u \rightarrow k\sigma_g$ and $3\sigma_u \rightarrow k\sigma_g$ photoionization channels of CO_2: —, $1\pi_u \rightarrow k\sigma_g$ channel; - - -, $3\sigma_u \rightarrow k\sigma_g$ channel.

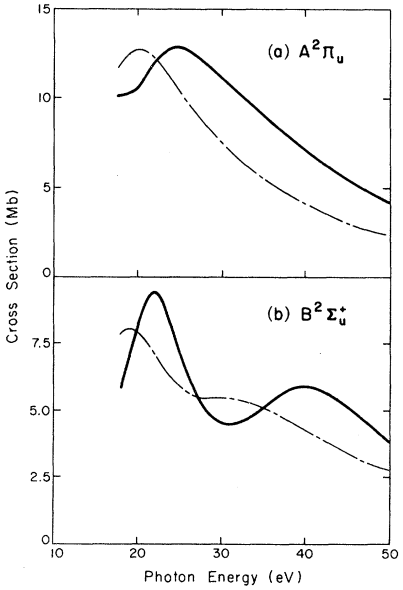

FIG. 7. Comparison of different theoretical cross sections for the production of the $A\,^2\Pi_u$ and $B\,^2\Sigma_u^+$ states of CO_2^+: —, present single-center FCHF results; — - — -, FCHF results obtained using the STMT approach (Ref. 1).

In Fig. 8 we present the computed asymmetry parameters for the $A\,^2\Pi_u$ and $B\,^2\Sigma_u^+$ channels. The present results are compared with those of the CMSM method and with experimental results. The agreement between the two theoretical calculations is fairly good, and both results agree fairly well with experimental results except for the 40.8-eV measurement of Katsumata *et al.*[17] in the $B\,^2\Sigma_u^+$ channel.

In Fig. 9(a) we compare the sum of our $A\,^2\Pi_u$ and $B\,^2\Sigma_u^+$ cross sections with the experimental results of Gustafsson *et al.*[12] and of Brion and Tan.[11] Due to the small difference between the IPs of these two states, neither of these two continuous-source photoelectron experiments resolved the individual branching ratios for these two channels. The Schwinger results are seen to agree fairly well with the experimental data for photon energies above 24 eV. Below 24 eV the computed cross section is too small. This error must be due to final-state correlation effects as we discussed earlier.

The total valence-shell cross sections are given in Fig. 9(b). Here we have summed the four theoretical cross sections leading to the $X\,^2\Pi_g$, $A\,^2\Pi_u$, $B\,^2\Sigma_u^+$, and $C\,^2\Sigma_g^+$ states of CO_2^+ given above and compare them to the sum of the experimental cross sections leading to these four states given by Brion and Tan.[11] The feature at a photon energy of 21 eV is again apparent in the experimental cross section and not in the theoretical cross section. The other major discrepancy between theory and experiment is the shoulder at 42 eV in the theoretical cross section due to the resonance in the $C\,^2\Sigma_g^+$ channel. As noted earlier, the magnitude of this feature would be reduced somewhat by vibrational averaging.

B. *K*-shell photoionization

As we have seen in Sec. III A, photoionization from the outer valence shell of CO_2 is fairly well represented by the use of the FCHF final-state approximation. Photoionization from the inner valence orbitals ($3\sigma_g, 2\sigma_u$) should be strongly affected by final-state correlation. This breakdown of the single-particle picture for the inner valence ionic states has been discussed by Domcke *et al.*[27] However, the *K*-shell photoionization should be fairly well described by the simple hole states used in the FCHF model.

We have computed the oxygen and carbon *K*-shell photoionization cross section of CO_2. The *K*-shell IPs were taken to be 297.5 eV for carbon and 541.1 eV for oxygen.[28] Since the initial-state correlated wave function discussed in Sec. II B does not include any correlation effects involving

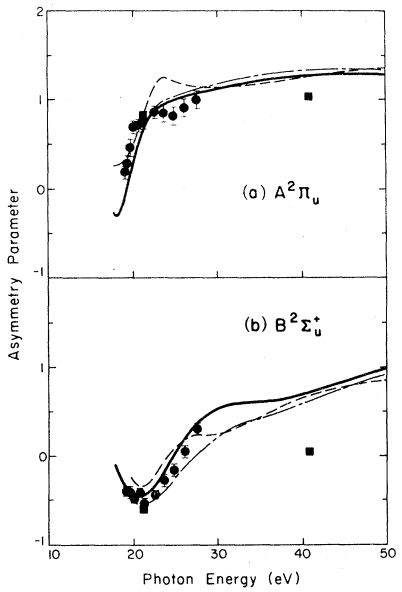

FIG. 8. Photoelectron asymmetry parameters for photoionization leading to the $A\,^2\Pi_u$ and $B\,^2\Sigma_u^+$ states of CO_2^+, see Fig. 4 for definitions of lines and symbols.

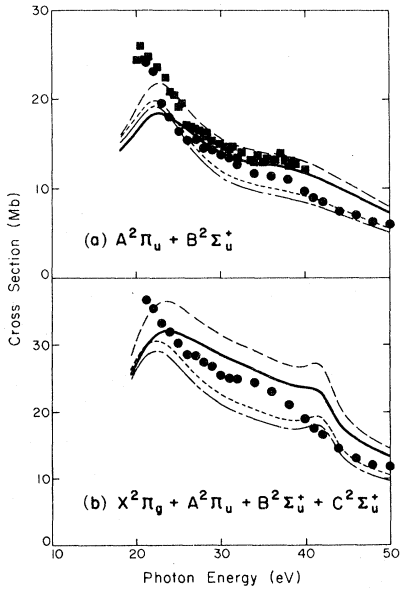

FIG. 9. Total photoionization cross sections for the production of the $A\,^2\Pi_u + B\,^2\Sigma_u^+$ and $X\,^2\Pi_g + A\,^2\Pi_u + B\,^2\Sigma_u^+ + C\,^2\Sigma_g^+$ states of CO_2^+, see Fig. 1 for definitions of lines and symbols.

the K-shell electrons, we have only computed the HFL and HFV forms of the photoionization cross section.

In Fig. 10(a) we present the computed carbon K-shell photoionization cross section of CO_2. We have compared the present theoretical results to those of Padial *et al.*[1] obtained using the STMT method and to the experimental energy-loss cross sections of Wight and Brion.[15] The Schwinger and STMT results are in good mutual agreement with both cross sections, showing a pronounced peak due to a $2\sigma_g \rightarrow k\sigma_u$ shape resonance. Both of the FCHF level theoretical results are seen to be in only rough agreement with the experimental data, which shows evidence of strong final-state correlation effects (e.g., shake-up states). In Fig. 10(b) we give the computed photoelectron asymmetry parameters which show a strong feature around a photon energy of 304 eV due to the $2\sigma_g \rightarrow k\sigma_u$ shape resonance.

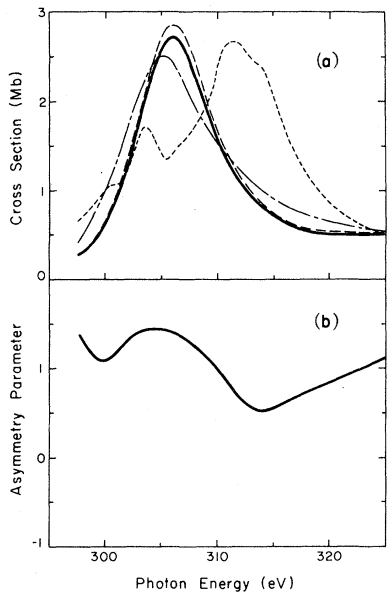

FIG. 10. Photoionization cross sections and photoelectron asymmetry parameters for carbon K-shell photoionization in CO_2: —, present results using the dipole length approximation and the HF initial-state wave function; — — —, present results using the dipole velocity approximation and the HF initial-state wave function; — - —-, results obtained using the STMT approach (Ref. 1); - - -, experimental results of Wight and Brion (Ref. 15). We have subtracted from the arbitrarily normalized cross sections of Ref. 15 a background term taken to be the cross section at 294 eV and scaled the result to agree with the theoretical HFL cross section at 325 eV. Notice that the theoretical length and velocity results for the photoelectron asymmetry parameters are nearly identical and we thus only present the length form.

The photoionization cross section for the oxygen K-shell is given in Fig. 11. The theoretical cross section we have presented is the sum of the cross sections for photoionizing electrons out of the nearly degenerate $1\sigma_g$ and $1\sigma_u$ molecular orbitals of CO_2. The effect of the narrow-shape resonance in the $1\sigma_g \rightarrow k\sigma_u$ channel is evident at a photon energy of 560 eV. We have compared our cross sections to the experimental absorption measurements of Barrus *et al.*[16] and to the STMT results of Padial *et al.*[1] The broad feature in the experimental cross section at a photon energy of 560 eV seems to be due in part to the shape resonance in the $1\sigma_g \rightarrow k\sigma_u$ channel. However, the fixed-nuclei FCHF model gives a much narrower width to this feature. Vibrational averaging would tend to broaden this peak within the FCHF approximation. The shoulder in the experimental cross section at 554 eV is not found using the FCHF approximation and is thus probably due to final-state correlation. The STMT results of Padial *et al.*[1] do not show the narrow resonance which is present in this system in the FCHF approximation. In the STMT cross section, the oscillator strength from the resonance has been smeared out over a large energy range in much the same manner as the

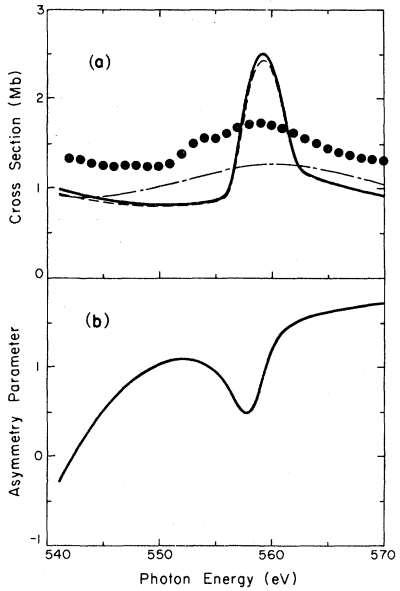

FIG. 11. Photoionization cross sections and photoelectron asymmetry parameters for oxygen K-shell photoionization in CO_2. See Fig. 10 for definitions of the lines: ●, absolute photoabsorption cross sections of Barrus *et al.* (Ref. 16).

$C\,^2\Sigma_g^+$ cross section was unphysically smoothed out by the STMT method.[9] The computed asymmetry parameters for this channel are given in Fig. 11(b). The effects of the shape resonance are once again clearly evident.

IV. CONCLUSION

Accurate fixed-nuclei FCHF photoionization cross sections of CO_2 have been presented. Comparison of the present results with those of the STMT[1] and CMSM[2,3] methods have shown that both the STMT and CMSM methods provide useful qualitative information about the cross sections but these methods can fail to reproduce some important features in photoionization cross sections. The present results have been found to be in reasonably good agreement with experimental data. Comparison of experimental and computed cross sections for the $A\,^2\Pi_u$ and $B\,^2\Sigma_u^+$ channels has yielded indirect evidence of a possible autoionization feature at a photon energy of 21 eV. These results also provide direct evidence of narrow-shape resonances in those partial channels where the continuum electron has σ_u symmetry. The effects of these resonances on differential photoionization cross sections has been computed to be substantial. Such shape resonances can also be expected to exhibit strong non-Franck-Condon vibrational effects. Both vibrational effects and autoionization can be studied using FCHF continuum wave functions such as those obtained here and will be the subject of future research.

ACKNOWLEDGMENTS

We want to thank T. A. Carlson for making available to us experimental asymmetry parameters prior to publication. One of us (R. R. L.) acknowledges support from an Exxon Foundation Graduate Educational Fellowship. This material is based upon work supported by the National Science Foundation under Grant No. CHE80-40870 The research reported in this paper made use of the Dreyfus-NSF Theoretical Chemistry Computer which was funded through grants from the Camille and Henry Dreyfus Foundation, the National Science Foundation (Grant No. CHE78-20235), and the Sloan Fund of the California Institute of Technology. We also thank Dr. W. Domcke for helpful discussions concerning our results.

[1]N. Padial G. Csanak, B. V. McKoy, and P. W. Langhoff, Phys. Rev. A 23, 218 (1981).
[2]J. R. Swanson, D. Dill, and J. L. Dehmer, J. Phys. B 13, L213 (1980).
[3]J. R. Swanson, D. Dill, and J. L. Dehmer, J. Phys. B 14, L207 (1981).
[4]R. R. Lucchese, G. Raseev, and V. McKoy, Phys. Rev. A (in press).
[5]R. R. Lucchese, D. K. Watson, and V. McKoy, Phys. Rev. A 22, 421 (1980).
[6]R. R. Lucchese and V. McKoy, Phys. Rev. A 24, 770 (1981).
[7]R. R. Lucchese, K. Takatsuka, D. K. Watson, and V. McKoy, in *Proceedings of the Symposium on Electron-Atom and Molecule Collisions, Universität Bielefeld, Germany, 1980,* edited by J. Hinze (Plenum, London and New York, 1981).
[8]F. Grimm, T. A. Carlson, W. B. Dress, P. Agron, J. O Thomson, and J. W. Davenport, J. Chem. Phys. 72, 3041 (1980).
[9]R. R. Lucchese and V. McKoy, J. Phys. Chem. 85, 2166 (1981).
[10]R. R. Lucchese and V. McKoy (unpublished).
[11]C. E. Brion and K. H. Tan, Chem. Phys. 34, 141 (1978).
[12]T. Gustafsson, E. W. Plummer, D. E. Eastman, and W. Gudat, Phys. Rev. A 17, 175 (1978).
[13]L. C. Lee, R. W. Carlson, and D. L. Judge, J. Phys. B 9, 855 (1976).
[14]R. W. Carlson, D. L. Judge, and M. Ogawa, J. Geophys. Res. 78, 3194 (1973).
[15]G. R. Wight and C. E. Brion, J. Electron Spectrosc. Relat. Phenom. 3, 191 (1974).
[16]D. M. Barrus, R. L. Blake, A. J. Burek, K. C. Chambers, and A. L. Pregenzer, Phys. Rev. A 20, 1045 (1979).
[17]S. Katsumata, Y. Achiba, and K. Kimura, J. Electron Spectrosc. Relat. Phenom. 17, 229 (1979).
[18](a) T. A. Carlson, M. O. Krause, F. A. Grimm, J. D. Allen, Jr., D. Mehaffy, P. R. Keller, and J. W. Taylor, Phys. Rev. A 23, 3316 (1981): (b) F. A. Grimm, J. D. Allen, Jr., T. A. Carlson, M. O. Krause, D. Mehaffy, P. R. Keller, and J. W. Taylor (unpublished).
[19]J. D. Weeks, A. Hazi, and S. A. Rice, in *Advances in Chemical Physics,* edited by I. Prigogine and S. A. Rice (Interscience, New York, 1969), Vol. XVI, p. 283.

[20]F. W. Bobrowicz and W. A. Goddard III, in *Methods of Electronic Structure Theory,* edited by H. F. Schaefer III (Plenum, New York, 1977), p. 79.
[21]T. H. Dunning, Jr., and P. J. Hay, in *Methods of Electronic Structure Theory,* edited by H. F. Schaefer III (Plenum, New York, 1977), p. 1.
[22]D. W. Turner, C. Baker, A. D. Baker, and C. R. Brundle, *Molecular Photoelectron Spectroscopy* (Wiley, London, 1970).
[23]J. R. Swanson and L. Armstrong, Jr., Phys. Rev. A 15, 661 (1977).
[24]H. P. Kelly, Chem. Phys. Lett. 20, 547 (1973).
[25]J. B. Rose and V. McKoy, J. Chem. Phys. 55, 5435 (1971).
[26]J. A. R. Samson and J. L. Gardner, J. Geophys. Res. 78, 3663 (1973).
[27]W. Domcke, L. S. Cederbaum, J. Schirmer, W. von Niessen, C. E. Brion, and K. H. Tan, Chem. Phys. 40, 171 (1979).
[28]K. Siegbahn, C. Nordling, G. Johansson, J. Hedman, P. F. Heden, K. Hamrin, U. Gelius, T. Bergmark, L. O. Werme, R. Manne, and Y. Baer, *ESCA Applied to Free Molecules* (North-Holland, Amsterdam, 1969).